Towards a Universal Veering Profile for Turbulent Ekman Flow at arbitrary Reynolds number

LES and DNS of Turbulent Ekman Flow

Draft January 2, 2021

Abstract

An analytical formulation for the profiles of stream- and span-wise velocity in turbulent Ekman flow is developed based on asymptotic theory as well as data from direct numerical simulation and large-eddy simulation. The profile of the stream-wise component follows the classical viscous, logarithmic and wake scaling. The span-wise component poses a conceptual challenge to the channel-flow analogy in the context of asymptotic mixing, and it exhibits a mixed scaling in the surface layer, but follows outer scaling for most of the outer layer. In the outer layer, the velocity component profiles can be described by an Ekman-spiral with adapted boundary conditions that result in a reduction of the spiral-like rotation.

1 Introduction

The exact veering of the wind away from its geostrophic direction is due to direct and indirect (due to turbulence) frictional effects, and it plays a role for various practical problems: It sets the amount of cross-isobaric volume flow and is thus a key factor in the life-cycle of large-scale synoptic systems. This mechanism is commonly referred to as 'Ekman pumping' referring to the perturbation of the geostrophic equilibrium that causes the veering as it was first described and solved for analytically by Ekman [1905]. On the mesoscale, shear in the surface layer is known to be crucial for the initiation and sustainment of strong convective events (REFERENCE?). And locally, directional sheer of the wind in the upper part of the surface layer may cause a yaw for large wind power generation devices (REFERENCE?).

The drag law for Ekman flow, including prediction of surface veering, has received considerable attention in the past.

- Rossby and Montgomery [1935] first approach;
- Tennekes [1973], Blackadar and Tennekes [1968] asymptotic similarity;
- Spalart [1989], Spalart et al. [2008, 2009] seminal LES studies in search for a universal log-law;
- Ansorge and Mellado [2014], Ansorge [2019] re-evaluation of the constants with geophysical focus;
- Högström [1988, 1996] (re-)consideration of observational data.

Attempts were also undertaken to obtain profiles of the wind speed: Gryning et al. [2007] present an extension of the wind-speed profile beyond the surface layer using a neutral referece profile and a stability correction; Kelly and Gryning [2010], based on a probabilistic representation of stratification, develop a model for the long-term mean windspeed in the atmospheric boundary layer and compare this with observation at different sites; Kelly and Troen [2016] demonstrate

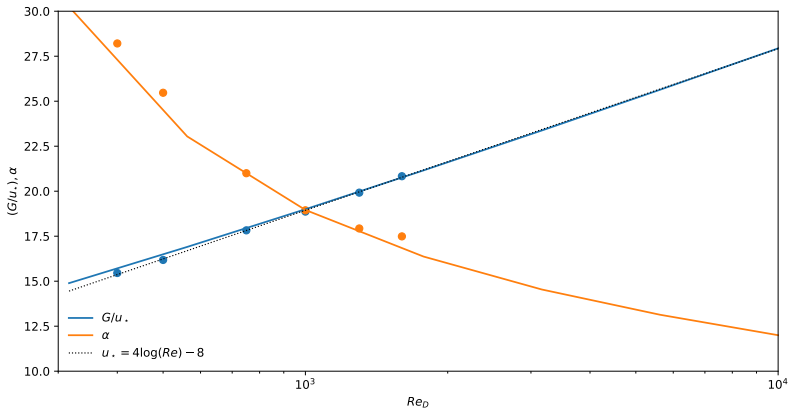

Figure 1: Variation of $Z_\star$ and surface veering with Reynolds number according to the theory by Spalart et al. (1989) and as estimated from DNS data

the effect of such improved model for wind-energy applications. These investigations merely focus on the wind speed and thus do not regard the actual vector, i.e. the veering of the wind with height is not described and there is little knowledge on the profile of the span-wise velocity component and the precise shape of the hodograph in the limit of a truly neutral Ekman boundary layer. While this is indeed an academic problem, the Ekman boundary layer often serves as limit for stratified boundary layers and thus not only needs to be understood but also well-described as reference for higher-order approaches that take into account possible effects of stratification, roughness or other physical complications of the geophysical system.

2 Formulation

We consider here incompressible, turbulent Ekman flow, that is, the turbulent flow over a flat rotating plate, as a physical model for the truly neutral atmospheric boundary layer (ABL). The f-plane approximation is applied such that rotation only acts on horizontal velocity components; we thus neglect rotational effects on the horizontal components of velocity and dynamical effects due to latitudinal variation of the rate of rotation.

The dimensional velocity vector of the numerical simulations is $\underline{U} = (U_1, U_2, U_3) = (U, V, W)$ over the coordinate system $Oxyz$, where an approximate alignment (plus/minus few degrees centigrade) of the direction Ox with the surface shear stress is achieved. The coordinate O_y points away from the wall, and Oz points in the span-wise direction normal to Oxy. For analysis of the results, we use two coordinate systems that are (i) exactly aligned with the surface shear stress and labelled by an upper index α as in $\underline{U}^\alpha$ for the velocity vector, and (ii) the coordinate system aligned with the free-atmosphere geostrophic wind labelled by an upper index G as in $\underline{U}^G$. We denote by $u_\star$ the modulus surface friction velocity and let $Z_\star = 1/u_\star$ for brevity.

3 Towards a Universal Velocity Profile for the Turbulent Ekman Layer

3.1 Drag-Law

Formulation of a drag-law for Ekman flow consists estimation of two key parameters in the flow as a function of Reynolds number. First, the modulus of the surface friction normalized by the geostrophic wind forcing, $u_\star$ and, second, the direction of surface shear stress, α, also termed wind veering. A non-zero veering of the wind is a rather special case in comparison with most turbulent flows conisdered in an engineering context, and it confronts us with a situation

where the most appropriate coordinate system for analysis (namely that aligned with the surface shear stress) is a priori unknown. We compare our DNS data against a semi-empirical based on integral consideration Spalart [1989] and find, as demonstrated in previous work Ansorge and Mellado [2014] excellent agreement in the range $400 < \mathbf{Re} < 1600$, representing a factor of 16 in variation of viscosity. [Add LES points]

We also find that the solution of the transient equation involved in estimation of $u_\star$ for a given Reynolds number Re_D is approximated reasonably by the formulation

$$u_\star = 4\log(\mathbf{Re}_D)) - 8 \tag{1}$$

which quantifies the 'weak' dependence of $u_\star$ on the Reynolds number as an approximately logarithmic one.

3.2 Stream-wise Velocity Component

For the stream-wise velocity profile (that in non-rotating flows due to the geometry is always aligned with the surface shear stress), well-established theories exist for various regimes according to their distance from the wall and the relative role of viscosity, turbulence and interaction with the outer region of the flow with the logarithmic law for the mean velocity as a central anchor point:

- In immediate vicinity to the surface, local turbulent mixing cannot occur for the no-slip/no-penetration boundary condition, and the mean velocity is described by a viscous profile of the form

  $$(U, W)^{\alpha+} = (z^+, 0) \tag{2a}$$

  where the direction of in absence of roughness elements are marginal linear regime / viscous sub-layer Foken [2002], Foken et al. [1978]. This viscous law has no degree of freedom given the drag-law defining surface friction and veering. Theoretical foundation is lacking for the exact shape of the velocity profile in the buffer layer; though crucial for turbulence production, it is commonly understood as a transition region between the linear profile at the surface and the logarithmic profile aloft. A pure blending from the linear velocity profile into the logarithmic one is, however, not reasonable as both the linear and logarithmic profile overestimate the velocity in the buffer layer. We therefore introduce a higher-order compensating term into the linear profile before blending it into the logarithmic law:

  $${U^\alpha_{\text{inner}}}^+ = \frac{y^+ + \gamma_4 (y^+)^4 + \gamma_6 (y^+)^6}{1 + \gamma_6 / u_{ref} (y^+)^6}, \tag{2b}$$

  where the fourth- and sixth-order terms in the nominator are designed to fit the profile below $y^+ \approx 10$ and the sixth-order correction in the denominator limits the growth of u_{inner} for large y^+.

- In the logarithmic region, we use the profile

  $${U^\alpha_{\log}}^+ = \frac{1}{\kappa} \log y^+ + C \tag{2c}$$

  with $\kappa = 0.416$ and $C = 5.4605$.

- The super-geostrophic maximum of streamwise velocity and a secondary minimum aloft the bulk-turbulent part of the boundary layer are well-described by a classic Ekman spiral with adapted boundary conditions and a shift in reference height.

Existing theories applied to the boundary layer:

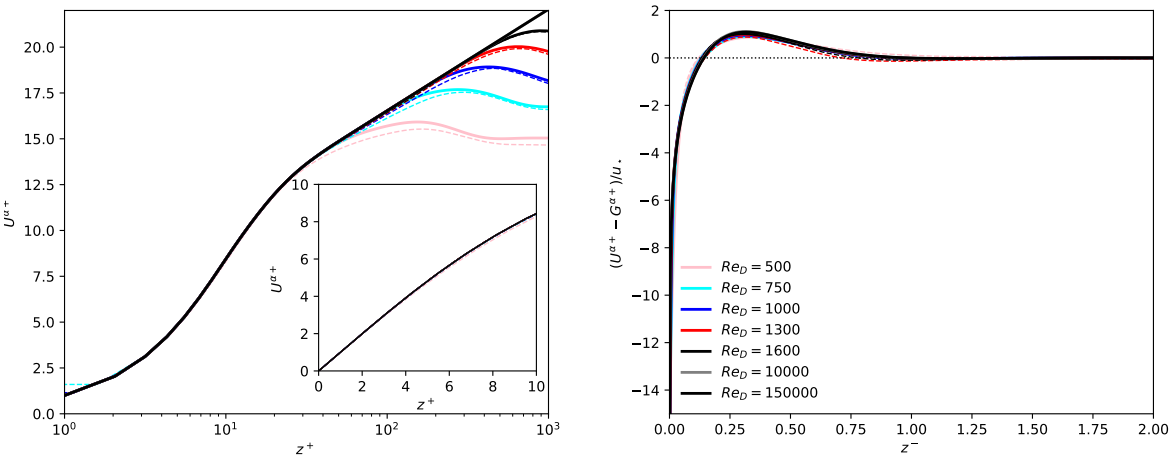

Figure 2: Shear-aligned profiles of velocity components $U^{\alpha+}$ in inner (left) and outer (right) units.

- Etling [2002], Emeis [2018] (Sec. 21.10; Eq. 21.48) – ad-hoc matching at Prandtl-layer height; requires α
- Emeis et al. [2007] (Sec. 3; Eq. 3.1-3.19) – 1D profile; considering constant (?) veering
- Gryning et al. [2007] (Mean wind profiles)

For non-rotating, non-external flows theoretical considerations by Townsend (cite to attached-eddy hypothesis) have recently been confirmed from both wind-tunnel experiments and numerical simulation Ng et al. [2011], Marusic et al. [2013] implying physical models for the second moments (Reynolds stresses) of the flow.

3.3 Span-wise velocity

The background rotation and associated veering of the surface wind implies a non-zero profile for the span-wise velocity that challenges the conventional assumptions related to the so-called channel-flow analogy: While the universal profiles in vicinity of the wall implies that the profile be zero or at least small with respect to the stream-wise component, the veering requires a value of $V_{top} = U_G \sin\alpha$ in the free stream (and thus also at the top of the boundary layer if we assume that substantial velocity gradients are confined to the turbulent part of the flow). This is commonly shown in terms of velocity hodographs aligned with the outer, geostrophic flow (cf. Fig. 4) and normalized by the geostrophic wind. Thus, the drag-law already implies three important properties of these hodographs, (i) the boundary conditions at the surface, (ii) the boundary condition at the top, and (iii) the inclination of the hodograph at the origin by the surface veering:

$$\underline{U}^G(z=0) = 0, \tag{3a}$$

$$\underline{U}^G(z \mapsto \infty) = \underline{G}^G = \begin{pmatrix} 1 \\ 0 \end{pmatrix} \tag{3b}$$

$$\left.\frac{\partial V^G}{\partial U^G}\right|_{z=0} = \sin\alpha \tag{3c}$$

Outer scaling of the velocity profile further implies that the velocity deficity of the spanwise component $V^\alpha - G^\alpha$ be a universal function of the outer height z^-, i.e.

$$V^\alpha - G^\alpha = f_V^\alpha(z^-). \tag{4}$$

Interpreting the shear-aligned spanwise velocity deficit $f_V^\alpha(z^-)$ as a signature of outer rotation may lead one to conclude that this universal function is appropriate down to the surface–irrespective of the Reynolds number. This cannot be the case for the variation of $f_V^\alpha(z^-)$ across the boundary layer (i.e. between $0 < z^- < 1$) must fulfill the drag law and boundary conditions; at the same time, the weak dependence of α and $u_\star$ on Re implies this range depends on Re.

Outer Layer. In the outer region of the flow (for $z^- \mapsto 1$), $f_V(z^-)$, should govern the spanwise velocity profile which indeed is supported by our DNS data (Fig.3): The deficit is close to zero for $z^- \gtrsim 1$, and can be approximated by a logarithmic profile in the range $0.15 \lesssim z^- \lesssim 0.4$. The slope of this profile is best fit by $\kappa_V = 0.836(1 + 150/Re_D)\kappa$, where the correction term for low Reynolds number may be omitted for $Re_D \gg 1000$. Based on Fig. 3, we pick the offset as a constant fraction (0.906) of $V_G^\alpha = Z_\star \sin\alpha$, i.e

$$V_{\log}(z^-) = \frac{1}{\kappa_V} \log\left(\frac{z^-}{0.4}\right) + 0.906 V_G^\alpha. \tag{5a}$$

The eventually converged simulations at intermediate Re_D (where the DNS could be run over several inertial periods) exhibit a super-geostrophic maximum (positiv velocity deficit) in the span-wise component. This maximum is not present or less pronounced for the simulations at higher Re where closer analysis reveals that the velocity profiles in the outer layer are still subject to a small though finite adaptation process on the inertial time scales $2\pi/f$ due to the relatively short time span for which these cases could be simulated. While there is no physical model for this wake region that leads to an analytical velocity profile formulation in the span-wise direction, an error-function transition from the outer logarithmic law to the boundary condition provides a reasonable fit:

$$V_{\text{outer}}(z^-) = (1 - w_V) V_{\log}(z^-) + w_V V_G^\alpha \tag{5b}$$

with

$$w_V = \frac{\operatorname{erf}\left[\xi_{\text{outer}} \log(z/z_{\text{ref}})\right] + 1}{2} \tag{5c}$$

where ξ_{outer} is a transition scale that defines the width of the wake region and z_{ref} defines the height. Based on the DNS data, we choose $\xi_{\text{outer}} = 2$ and let z_{ref} such that $V_{\log}(z_{\text{ref}}) = 0.98 V_G^\alpha$. There is, however, a degree of ambiguity in the exact choice of these parameters due to the imperfect convergence of the DNS data to the statistical equilibrium.

Inner Layer. It is important to note that the logarithmic layer observed here for the span-wise velocity does not conincide with the log-region of the streamwise velocity but is rather a 'continuation' through the outer layer. This is consistent with the recent finding of a second log-region in the outer region of Ekman flow (... et al. (incl. Sullivan), JAS 2019). Below this region, the gradients in span-wise velocity are rather small and the span-wise velocity monotonically approaches its surface boundary condition $V(z = 0) = 0$. While the stream-wise velocity follows a universal inner scaling that has acquired its universal, Re-independent shape for $Re_D > \mathcal{O}\left(10^3\right)$, the span-wise component that defines how the velocity vector veers when the surface is approached, does not collapse in inner units, and there is, most importantly no sign of convergence even at the highest Reynolds numbers for which simulations where carried out. Even though the simplest assumption $V = 0$ is reasonable for the lower part of the surface surface layer ($z^- < 10^{-3}$), it does not appropriately capture the profile in the rest of the surface layer:

First, $V = 0$ implies a discontinuity in the velocity profile at $z^- = 0.1$, where the outer scaling found above yields a finite value at geophysical Re, i.e. there is non-zero veering in the upper part of the surface layer–as is well-known also from field observation. Second, the

layer around $z^- = 0.1$ is crucial to obtain the characteristic and well-established shape of the hodographs as the layer where V sets in marks the 'maximum' of V^- vs. U^-. This illustrates that the higher-order (in terms of the channel-flow analogy where $V = 0$) correction follows a mixed scaling when the surface is approached which has been demonstrated for higher-order terms in other types of flow [Mellado et al., 2016].

The scale for the magnitude of the span-wise velocity component is $u_\star \sin\alpha$. Based on our DNS data, we suggest that the Reynolds number scaling of this velocity-magnitude scale is captured by $Re_\tau^{-1/2}$ which is indeed known from the generalization of higher-order statistics, such as turbulent fluxes in the inner layer [Marusic et al., 2013] that also follow a mixed scaling in the inner layer. We then parameterize the spanwise velocity at 10 wall units as anchor point in the inner layer:

$$V_{10} \equiv V(z^+ = 10) = 750 \frac{u_\star \sin\alpha}{\sqrt{Re_\tau}}. \tag{6a}$$

This leaves us with three fixed points of the velocity profile in the inner layer, namely (i) the boundary condition $V_0 = 0$, (ii) V_{10} at $z^+ = 10$, and (iii) the lower end of the logarithmic profile at $z^- = 0.1$ where the latter two are semi-empirically estimated from DNS data. In absence of well-established scaling considerations for the span-wise velocity, the choice of profile fits joining these three points is indeed arbitrary, but we can resort to the DNS data for an empirical approach and find that a square-root profile fits $V(z^+)$ in the surface layer. A linear profile for V is employed in the viscous sub-layer. Based on the physical extent of the viscous sub-layer in Ekman flow around five wall units [Foken, 2002, Ansorge, 2019], we choose $z^+ = 5$ to transition from one to the other and note that V is already very small at this height. The span-wise velocity profile in the surface layer is then estimated as

$$V(z^+)\big|_{\text{inner}} = \begin{cases} a_1 z^+ & ; \quad z^+ \leq 5 \\ b_1 + b_2\sqrt{z^+} & ; \quad 5 < z^+ < Re_\tau/10 \end{cases}, \tag{6b}$$

with b_1 and b_2 estimated such that

$$\begin{array}{rcl} V(z^+ = 10)\big|_{\text{inner}} & = & V_{10} \\ V(z^+ = Re_\tau/10)\big|_{\text{inner}} & = & V_{\text{outer}}(0.1) \end{array} \Rightarrow \begin{cases} b_2 = \dfrac{V_{\text{outer}}(0.1) - V_{10}}{\sqrt{Re_\tau/10} - \sqrt{10}} \\ b_1 = V_{10} - \sqrt{10} b_2 \end{cases} \tag{6c}$$

We then estimate α from the matching condition at $z^+ = 5$, i.e.

$$5a = b_1 + \sqrt{5} b_2 \Rightarrow a = \frac{1}{5}\left[V_{10} + (\sqrt{5} - \sqrt{10})\left(\frac{V_{\text{outer}} - V_{10}}{\sqrt{Re_\tau/10} - \sqrt{10}}\right)\right]. \tag{6d}$$

Matching region. While the profile composed of $V_{\text{inner}}(z^+ \leq 0.1Re_\tau)$, $V_{\text{outer}}(z^- > 0.1)$ is continuous, it is not smooth at $z^- = 0.1$, i.e. at the transition from power-law ($V \propto \sqrt{z^+}$) to logarithmic scaling. To alleviate this issue, we use a second-order polynomial for transition from the inner to the outer layer in the range $z_{\text{low}} < z < z_{\text{up}}$ such that

$$V_{\text{trans}}(z^-) = \qquad V_{\text{inner}}(z^+_{\text{low}}) + \Delta V\left(a z_{arg} + b(z_{arg})^2\right) \tag{6e}$$

with $\Delta V = V_{\text{outer}}(z^-_{\text{up}}) - V_{\text{inner}}(z^+_{\text{low}})$ and $z_{arg} = (z - z_{\text{low}})/(z_{\text{up}} - z_{\text{low}})$. It is $a + b = 1$ for $V_{\text{trans}}(z^-_{\text{up}}) = V_{\text{outer}}(z^-_{\text{up}})$, and we constrain a by

$$\left.\frac{\partial V_{\text{trans}}}{\partial z^-}\right|_{z=z_{\text{low}}} = \left.\frac{\partial V_{\text{inner}}}{\partial z^-}\right|_{z=z_{\text{low}}}, \tag{6f}$$

where we find that $z^-_{\text{low}} = 0.06$ and $z^-_{\text{up}} = 0.13$ yield satisfactory agreement with DNS data.

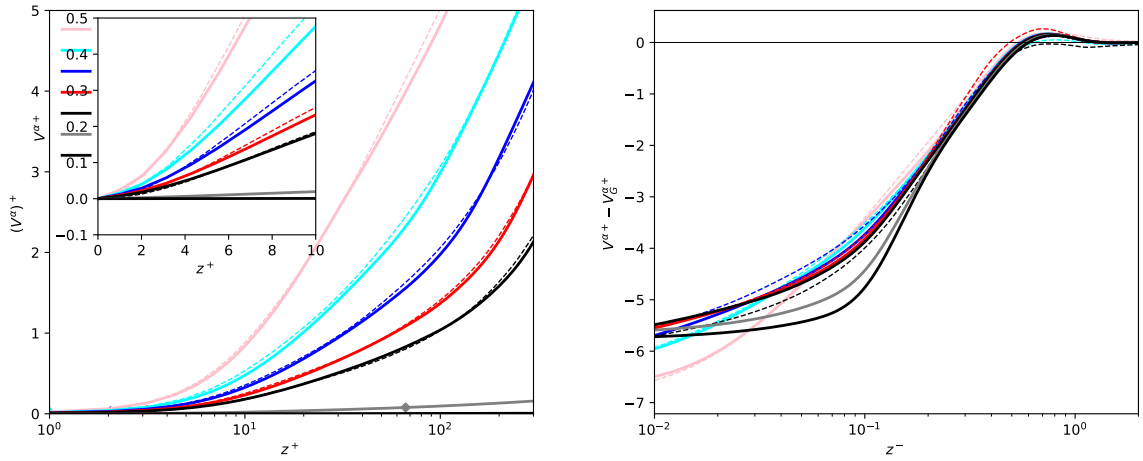

Figure 3: Profiles of shear-aligned span-wise velocity $(W^\alpha)^+$ versus inner and outer height. Dashed lines show DNS data, thick, opaque lines are from the semi-emprical theory developed above.

4 Comparison with other theories

Compare to Emeis (2002) and Gryning (2007); highlight explicit knowledge on veering-profile $\rightarrow$ directional sheer;

Implications for **K-theory** (we now can consider that shear and stress are not necessarily perfectly aligned). $\rightarrow$ can we do something to infer a K-profile from these theoretical considerations?

5 Conclusions

Applications:

- reference-shear for neutral profile approaches(systematic!) $\rightarrow$ wind engineering!
- initial condition for LES/DNS to eliminate/minimize inertial oscillation in Benchmark simulations
-

A Laminar Ekman solution with consideration of inner layer

$$\begin{pmatrix}\partial_t U\\ \partial_t W\end{pmatrix} = \begin{pmatrix} fW & + & \nu\partial_z^2 U\\ -f(U-G) & + & \nu\partial_z^2 W\end{pmatrix} \tag{7a}$$

$$\Rightarrow \partial_t(U+iW) = f(W-i(U-G)))+\nu\partial_z^2(U+iW) \tag{7b}$$

In stationary conditions, this system is solved by

$$\hat{u}(z) = U_{\text{inf}} + e^{-\gamma z}\left[A\cos\gamma z + B\sin\gamma z\right] \tag{7c}$$

$$\hat{w}(z) = W_{\text{inf}} + e^{-\gamma z}\left[-A\sin\gamma z + B\cos\gamma z\right] \tag{7d}$$

where the constants U_{inf}, W_{inf} set the top boundary condition and A and B set the bottom boundary condition. The most common boundary condition for a surface Ekman layer is $A =$

(a) **(b)** **(c)**

Figure 4: **(a)** Velocity deficity, **(b)** velocity profile in shear-aligned hodographs and **(c)** hodograph in geostrophy-aligned coordinates. Thick, solid lines show theory, dashed lines data from DNS.

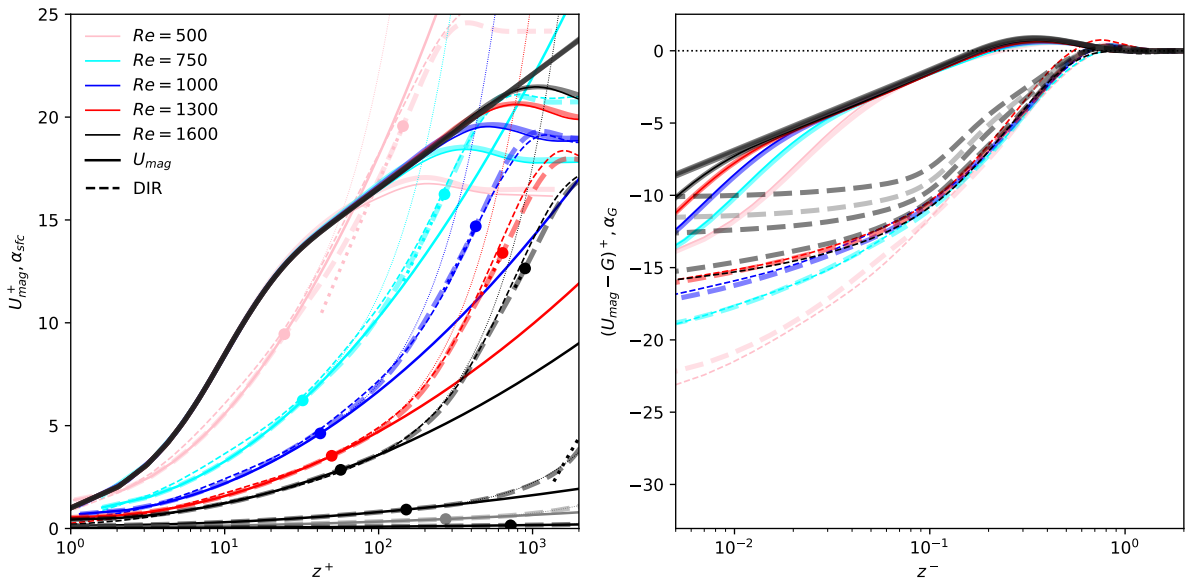

Figure 5: Total velocity and veering (in degrees) vs inner and outer height. Dashed lines show DNS data, thick lines are from semi-empirical theory.

$U_{\mathrm{inf}=G}$, $B = 0$, and $W_{\mathrm{inf}=0}$. The lower boundary condition, however, neglects the existence of the surface layer, and it appears reasonable to define $A = cG$ where $c < 1$ is a constant that icorporates the increased shear in the surface layer. Given a 'matching height' z_{match} and normalized matching height $\xi = \gamma z_{\mathrm{match}}$ in the upper part of the inner layer, we can match the Ekman profile to the inner layer by letting

$$\begin{aligned} u(z_{\mathrm{match}}) \equiv u_{\mathrm{match}} &= U_{\mathrm{inf}} + e^{-\xi}\left[A\cos\xi + B\sin\xi\right] \\ w(z_{\mathrm{match}}) \equiv w_{\mathrm{match}} &= W_{\mathrm{inf}} + e^{-\xi}\left[-A\sin\xi + B\cos\xi\right] \end{aligned} \tag{8}$$

$$e^{\xi}\begin{pmatrix} u_{\mathrm{match}} - U_{\mathrm{inf}} \\ w_{\mathrm{match}} - W_{\mathrm{inf}} \end{pmatrix} = \begin{pmatrix} \cos\xi A & +\sin\xi B \\ -\sin\xi A & +\cos\xi B \end{pmatrix} \tag{9}$$

$$\tag{10}$$

Matching the profile at $\xi = 0$, one obtains $A = \Delta u_{\mathrm{match}}$ and $B = -\Delta w_{\mathrm{match}}$. Otherwise, it is

$$e^{\xi}\Delta u_{\mathrm{match}} = A\cos\xi + B\sin\xi \tag{11a}$$

$$e^{\xi}(\cos\xi\Delta u_{\mathrm{match}} - \sin\xi\Delta w_{\mathrm{match}}) = A(\cos^2\xi + \sin^2\xi) \tag{11b}$$

$$\Rightarrow A = e^{\xi}(\cos\xi\Delta u_{\mathrm{match}} + \sin\xi\Delta w_{\mathrm{match}}) \tag{11c}$$

$$B = \frac{e^{\xi}\Delta u_{\mathrm{match}} - A\cos\xi}{\sin\xi} \tag{11d}$$

$$= e^{\xi}\frac{\sin^2\xi\Delta u_{\mathrm{match}} + \sin\xi\cos\xi\Delta w_{\mathrm{match}}}{\sin\xi} \tag{11e}$$

$$= e^{\xi}(\sin\xi\Delta u_{\mathrm{match}} + \cos\xi\Delta w_{\mathrm{match}}) \tag{11f}$$

References

Cedrick Ansorge. Scale Dependence of Atmosphere–Surface Coupling Through Similarity Theory. *Boundary-Layer Meteorol*, 170(1):1–27, 2019.

Cedrick Ansorge and Juan-Pedro Mellado. Global Intermittency and Collapsing Turbulence in the Stratified Planetary Boundary Layer. *Boundary-Layer Meteorol*, 153(1):89–116, July 2014.

A K Blackadar and Hendrik Tennekes. Asymptotic Similarity in Neutral Barotropic Planetary Boundary Layers. *J Atmos Sci*, 25:1015–1020, November 1968.

Vagn Walfrid Ekman. On the influence of the earth's rotation on ocean currents. *Ark. Mat. Astron. Fys., Vol. 2 (1905), pp. 1-53*, 2:1–53, 1905.

Stefan Emeis. *Wind Energy Meteorology*. Atmospheric Physics for Wind Power Generation. Springer, Heidelberg, 2 edition, March 2018.

Stefan Emeis, Kathrin Baumann-Stanzer, Martin Piringer, Margarita Kallistratova, Rostislav Kouznetsov, and Vladislav Yushkov. Wind and turbulence in the urban boundary layer analysis from acoustic remote sensing data and fit to analytical relations. *Met Zet*, 16(4): 393–406, 2007.

Dieter Etling. *Theoretische Meteorologie*. Eine Einführung. Springer-Verlag, Berlin, Heidelberg, 2nd edition, 2002.

Thomas Foken. Some aspects of the viscous sublayer. *Met Zet*, 11(4):267–272, 2002.

Thomas Foken, S A Kitajgorodskij, and O A Kuznecov. On the dynamics of the molecular temperature boundary layer above the sea. *Boundary-Layer Meteorol*, 15(3):289–300, November 1978.

Sven-Erik Gryning, Ekaterina Batchvarova, Burghard Brümmer, Hans Jørgensen, and Søren Larsen. On the extension of the wind profile over homogeneous terrain beyond the surface boundary layer. *Boundary-Layer Meteorol*, 124(2):251–268, 2007.

Ulf Högström. Non-dimensional wind and temperature profiles in the atmospheric surface layer: A re-evaluation. *Boundary-Layer Meteorol*, 42:55–78, 1988.

Ulf Högström. Review of some basic characteristics of the atmospheric surface layer. *Boundary-Layer Meteorol*, 78(3-4):215–246, March 1996.

Mark Kelly and Sven-Erik Gryning. Long-Term Mean Wind Profiles Based on Similarity Theory. *Boundary-Layer Meteorol*, 136(3):377–390, September 2010.

Mark Kelly and Ib Troen. Probabilistic stability and 'tall' wind profiles: theory and method for use in wind resource assessment. *Wind Energy*, 19(2):227–241, February 2016.

Ivan Marusic, Jason P Monty, Marcus Hultmark, and Alexander J Smits. On the logarithmic region in wall turbulence. *J Fluid Mech*, 716, February 2013.

Juan-Pedro Mellado, Chiel C van Heerwaarden, and Jade Rachele Garcia. Near-Surface Effects of Free Atmosphere Stratification in Free Convection. *Boundary-Layer Meteorol*, 159(1):69–95, 2016.

H C H Ng, Jason P Monty, N Hutchins, M S Chong, and Ivan Marusic. Comparison of turbulent channel and pipe flows with varying Reynolds number. *Exp Fluids*, 51(5):1261–1281, June 2011.

Carl-Gustaf Rossby and Raymond B Montgomery. The layer of frictional influence in wind and ocean currents. *Papers in Physical Oceanography and Meteorology*, III(3):1–101, 1935.

Philippe R Spalart. Theoretical and numerical studies of a three-dimensional turbulent boundary layer. *J Fluid Mech*, 205:319–340, 1989.

Philippe R Spalart, Gary Neil Coleman, and Roderick Johnstone. Direct numerical simulation of the Ekman layer: A step in Reynolds number, and cautious support for a log law with a shifted origin (Retracted article. See vol. 21, art. no. 109901, 2009). *Phys Fluids*, 20(10): 101507, 2008.

Philippe R Spalart, Gary Neil Coleman, and Roderick Johnstone. Retraction: "Direct numerical simulation of the Ekman layer: A step in Reynolds number, and cautious support for a log law with a shifted origin" [Phys. Fluids 20, 101507 (2008)]. *Phys Fluids*, 21(10):109901, 2009.

Hendrik Tennekes. The Logarithmic Wind Profile. *J Atmos Sci*, 30:234–238, March 1973.